PET/MRI for Cardiac Imaging: Technical Considerations and Potential Applications

3

Stephan G. Nekolla, Christoph Rischpler, and Karl P. Kunze

3.1 Introduction

To investigate the potential role of cardiac PET/MRI, it is useful to consider the clinical and economical boundary conditions in cardiac imaging. Two factors have a large influence: Firstly, the overwhelming mainstay of nuclear cardiology is SPECT imaging. It is an easy-to-perform methodology with a high clinical utility, and considerable activities are ongoing to reduce the clinical examination times as well as exposition to ionizing radiation [1, 2].

Secondly, as published by The Task Force on Myocardial Revascularization of the European Society of Cardiology (ESC) and the European Association for Cardio-Thoracic Surgery (EACTS), the recent guidelines on myocardial revascularization consider several cardiac imaging approaches (stress echo, SPECT, PET, and MRI perfusion) *equally* suitable for the diagnosis of patients with suspected coronary artery diseases (CADs) with an intermediate pretest probability [3]. Although this strictly represents the European perspective, it is anticipated that this situation will apply worldwide as well. Fortunately, the same document introduces hybrid imaging for the first time and classifies it as IIa ("should be considered"). This primarily reflects the incremental value of adding (morphological) information derived from CT to perfusion data generated with nuclear imaging [4]. However, a common observation in hybrid imaging systems is an increased complexity of the workflow, which may result in a higher susceptibility to errors. Regarding the disproportionately higher complexity of MR compared to CT, it is clear that this is a relevant issue for integrated PET/MRI systems.

S.G. Nekolla, PhD (✉) • C. Rischpler, MD • K.P. Kunze, MSc
Nuklearmedizinische Klinik und Poliklinik, Klinikum rechts der Isar, Technische Universität München, Munich, Germany
e-mail: stephan.nekolla@tum.de

T.H. Schindler et al. (eds.), *Molecular and Multimodality Imaging in Cardiovascular Disease*, DOI 10.1007/978-3-319-19611-4_3

So, what does this mean specifically for cardiac PET/MRI? At the time of writing this chapter, the number of review articles and book chapters outnumbers those of actual research articles (taking case studies out of the focus for the moment) and is small even if compared to the very modest number of PET/MRI systems installed since 2010 which is estimated to be slightly above 50. Still, the aspects favoring MRI such as the higher soft tissue spatial resolution, the lack of ionizing radiation, and the better tolerable contrast agents hold true. Those aspects are supplemented with the high rate of technological innovations in cardiac MRI such as perfusion imaging and T1 mapping [5, 6]. Integrating all these results in an approach where the fact that PET/MRI is not a sequential technique but allows fully parallel imaging offers a time-effective methodology with *both* modalities acquiring simultaneously what they can do in a reliable manner. Examples would be highly specific PET probes (e.g., innervation and/or inflammation) combined with MRI delineating anatomical references, perfusion, or tissue with an altered volume of distribution for contrast media in complex cardiac pathophysiologies, for which high throughput and low costs are not the limiting factors.

This chapter tries to provide insights on the technical aspects, investigate available applications, and target its potential strengths especially in nonstandard applications beyond conventional perfusion and viability imaging.

3.2 Technical Considerations

A fully integrated PET/MRI system is a complex technology as the combination of high static magnetic fields, variable gradient fields, and powerful radiofrequency in the range of several kilowatts would interact with conventional photomultiplier tubes and the PET electronics. In the other direction, PET-related components cause inhomogeneities in the magnetic fields, and electromagnetic interferences could result in a degradation of the MR image quality. To date, three different constructions of PET/MRI systems are available and regulatory approved. A sequential design aligns the PET and MR components axially and connects with the patient bed on a rail system (Ingenuity TF PET/MRI, Philips, Best, the Netherlands) [7]. The first truly integrated device with simultaneous MR and PET acquisitions was the Biograph mMR (Siemens Healthcare, Erlangen, Germany) [8]. This device uses avalanche photodiodes (APDs) which are insensitive to the magnetic field [9]. Recently, a second integrated system, the SIGNA PET/MRI (General Electric Healthcare, Milwaukee, USA) was introduced. It uses silicon photomultiplier detectors (SiPM) enabling time-of-flight PET imaging [10, 11].

3.2.1 Attenuation Correction

A correct attenuation map is the cornerstone of PET quantification. Errors in this map result in significant deviations as shown in several studies where the misalignment between PET and CT was investigated (Fig. 3.1) [12, 13].

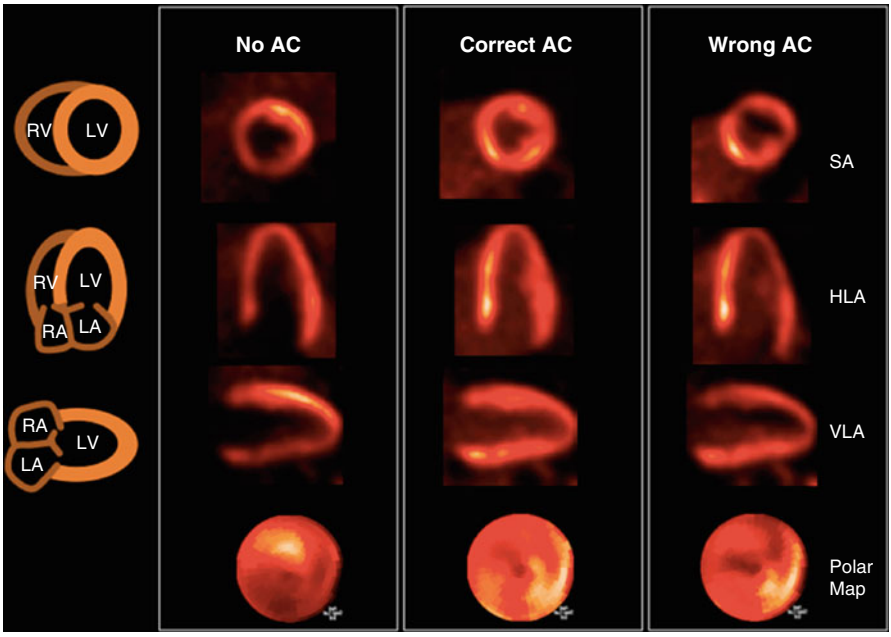

Fig. 3.1 Attenuation correction in cardiac PET. Attenuation correction is the cornerstone of quantification in PET imaging. Cardiac PET is especially prone to this as shown below. In contrast to cardiac SPECT where non-AC data are routinely used in the clinical reading, the effects in PET are much larger (*left column*). Even modest misalignment of 6 mm as shown in the right column alters the apparent tracer distribution

In stand-alone PET systems the attenuation map is generated by a rotating rod source, while in PET/CT systems the attenuation map is estimated from CT data. This adds to the total radiation exposure; however, using suitable protocols, values as low as using rotational sources can be achieved [14, 15]. Unfortunately, MRI is not able to directly retrieve the desired information as it has no access to the absorption of high-energy photons. We approached this problem by using tissue segmentation and assigning standardized, non-patient-specific attenuation values to the tissue classes (Fig. 3.2) [16].

As in stand-alone PET using rod sources, the cortical bone is ignored. The acquisition of these images requires usually about 18 s per bed position during one breath-hold. Alternatively, T1-weighted turbo spin-echo sequences are used with the advantage of a shorter acquisition time but combining fat and water into a single tissue class [17]. Obviously, the major disadvantage of the segmentation-based approach is the limited number of tissue classes especially if a significant inter-patient variability in lung structure and location could be anticipated. General disadvantages of this approach are that metal implants do not contribute to the attenuation map and that contrast agents may cause inaccuracies due to reduced T1 values (Fig. 3.3) [18]. However, this segmentation-based approach is currently used in commercially available PET/MRI scanners [16, 17], and our group has demonstrated a good correlation between PET/MRI

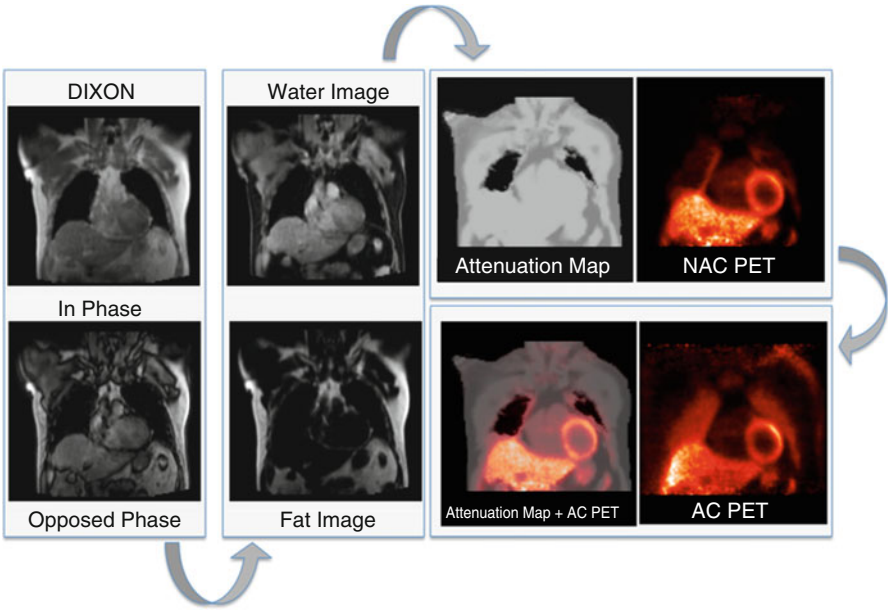

Fig. 3.2 Attenuation correction in PET/MR. The attenuation map is generated using in- and opposed-phase MR Dixon images from which fat and water images are computed. In the attenuation map air, lung, fat, and soft tissues are automatically segmented. Using this attenuation map and NAC (non-attenuation-corrected) PET data, the final AC PET images are calculated

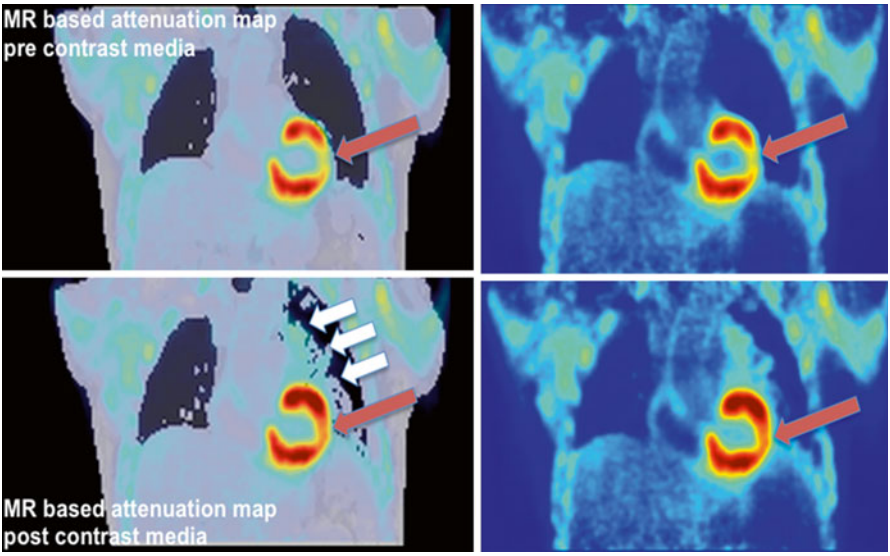

Fig. 3.3 AC pre/post KM. Dixon-based attenuation maps prior (*top left*) and after (*bottom left*) injection of contrast media shown together with reconstructions from the same PET scan but using the respective attenuation maps. Both PET data sets are scaled to the same maximum. Due to an overcorrection caused by the (apparent) larger amount of attenuating "lung" (*white arrows*) tissue, the myocardial PET values using the post-contrast attenuation maps differ (*red arrows*)

and PET/CT data in oncologic studies [19]. Initial work in cardiac patients has also shown good agreement between sequentially acquired patients with PET/CT and PET/MRI [20].

Another PET/MRI specific limitation, which affects attenuation correction, is the limited field of view (FOV) of the MR system potentially truncating the MR data. In other words, the PET scanner has a larger FOV as the MR system. This results in MR "invisible" tissue where body parts are outside the FOV introducing a bias in the attenuation correction. Thus, based on PET emission data, tissue is extrapolated and added to the map [21, 22]. A more desirable solution would be, however, the extension of the field of view, as was recently suggested and showed promising results [23].

Multiple components outside the body but inside the PET/MRI field of view, such as coils, positioning aids, monitoring devices, cables, earphones, and the – as compared to PET/CT, more massive – patient bed, are an additional source of photon scatter and attenuation. Most of these objects are MR "invisible" and are at rather random locations and thus do not necessarily contribute (although they should do) to the attenuation map. Only the patient bed and the fixed coils with known location are added to the final attenuation map [24–26]. As a result of this issue, vendors of such devices have redesigned them to reduce size and weight, but the effects are still measurable although small. If this has a relevant impact on the diagnostic performance, however, is not known yet. It might be anticipated that the effects are in the same order of objects overestimated in PET/CT imaging due to CT reconstruction artifacts or non-ferromagnetic signal voids in non-hybrid MR imaging.

A special group of artifacts in cardiac imaging arises from implantable devices. In difference to cardiac PET/CT and SPECT/CT, implantable cardiac devices (ICDs, CRT devices, or pacemakers) are of significant concern in MR imaging. As mentioned before, the devices cause CT artifacts, which potentially result in a biased attenuation correction, although initial work in PET/CT showed only little effects [27]. But in MRI, the effects are twofold. Nonmagnetic metals disturb the homogeneity of the magnetic field and cause signal voids, which clearly exceed the actual size of the object and thus underestimate the true attenuation. The second, more critical effect stems from an interaction with the radiofrequency and could cause life-threatening malfunction or local heating. Thus, many patients are excluded from MRI (including PET/MRI) which represents an increasing problem as the number of patients with diseases qualifying for the implantation of those devices is growing [28, 29]. Although newer generations of these devices are MR compatible, the logistical hurdles are significant and the procedures can be time-consuming. In general, it is advisable that the clinical reader is informed about potential sources of artifacts and a strict quality control with a special emphasis on correct alignment of MR-derived attenuation correction maps and PET data should be performed.

3.2.2 Imaging Workflow

We mentioned already that proper attenuation correction and exact alignment of the attenuation map is mandatory for correct diagnostic performance. Regarding this point, one major advantage of MR compared to CT is that the AC scan may be

repeated as often as necessary without any ionizing radiation. The subsequent choice of the optimal attenuation map, however, is rather time-consuming and thus inefficient and inconvenient. Recent developments in PET/CT, however, indicate that software-assisted solutions will become available soon [30, 31].

It is relevant to remember that considerations on PET/MRI workflows include the fact that most data are acquired in "parallel" and not "simultaneously." PET measures in volume rather than slice modes with variable frame lengths between seconds and up to 20–30 min (or more) depending on the chosen tracer, the uptake pattern and its half-life, the injected activity, and the patience of the patient. Thus, PET data integrates always the voluntary and involuntary patient motion (respiration, contractile motion, and "true" patient motion). This is in quite some difference to the MR acquisitions. As MR is so motion sensitive due to its image generation physics, MR data is usually acquired sequentially, with slice acquisition durations ranging from milliseconds for dynamic scans to several breath-holds for high-resolution images. It is inherent to sequential imaging that if data is acquired over several breath-holds, the limited reproducibility of the patient's breath-holding creates spatially somewhat inconstant images. This has an underestimated limitation that ungated (regarding the cardiac cycle and the ventilation) PET images are fused with spatiotemporal consistent MR images (e.g., end-diastole in expiration). Related to this, the reading process of PET/MRI data is more complex than typically found in PET/CT or SPECT/CT as PET volume data ultimately is mapped on various (partly overlapping) MR slices acquired in various positions and orientations (e.g., short axes; two-, three-, and four-chamber view). This is tedious, and the future will hopefully bring motion-triggered acquisition [32] or software corrections [33] in order to allow free-breathing imaging.

However, there are also applications that might benefit from truly simultaneous acquisition of PET and MR data. Potential workflows are depicted in Fig. 3.4. Synergistic benefits of integrating PET (with its vast variety of specific tracers, its good volume coverage) and MRI (with its high in-plane resolution) are rather compact protocols with a maximum of 30 min scan time. Today, clinical MRI in the heart is realistically a matter of 45–60 min, and all aspects of perfusion, contractile function, and metabolic surrogate parameters are measured sequentially. Thus, integrated PET/MRI could increase patient comfort and throughput and thus cost-effectiveness which potentially offset the significant more expensive costs of the device. Cardiovascular PET/MRI has the advantage that typically only a limited area in the body is investigated which reduces the scan time in difference to complex whole-body protocols in oncological imaging. However, simultaneous PET/MRI imaging is challenging from the operational perspective: it needs to be kept in mind that perfectly matching image data do not come automatically and considerable user interaction is needed. Compared with the highly automated workflows in PET/CT and SPECT/CT, this is a major limitation today. Finally, cross-training of the involved personnel operating the scanner is obligatory which holds also true for professionals planning and interpreting the scan. Consequently, a closer-than-usual collaboration between nuclear medicine physicians, radiologists, cardiologists, and physicists and technologists is mandatory.

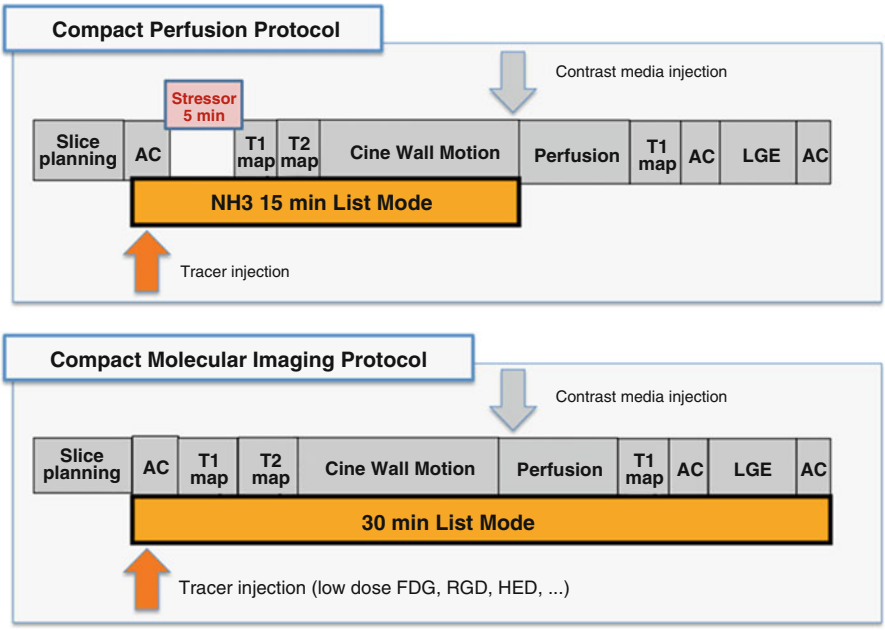

Fig. 3.4 Potential workflows (compact stress/rest perfusion, molecular imaging) for simultaneous PET/MRI

3.3 Cardiac Applications in PET/MRI

3.3.1 Myocardial Perfusion

Awhile being a fundamental advantage of cardiac PET, absolute quantification is one of the major limitations of MRI. MR signal intensities depend on a vast array of parameters such as imaging hardware (transmitters, receivers, amplifiers, gradients, coils, etc.), pulse sequences, as well as many other features which vary between vendors, magnetic field strengths, and scanner models (Fig. 3.4). Although usually irrelevant in morphological imaging, quantification of MR signal is an important step in dynamic MR imaging. Due to its superior time resolution, the true potential in quantitative MRI lies in dynamic data, even if this term is used somewhat differently as compared to nuclear medicine. Basically, it refers to a series of images, where either acquisition parameters varied (such as the inversion time in T1 mapping or the gradients in diffusion imaging) or – more familiar to nuclear cardiology – which are acquired after the injection of MR contrast media.

Perfusion imaging is, as mentioned earlier, a traditional domain of nuclear imaging for the diagnosis of a flow-limiting stenosis in coronary artery disease (CAD), and the investigation of the hemodynamic significance of known CAD is of high clinical relevance. There is increasing evidence that PET MPI offers advantages over the traditional SPECT-based approach due to the absolute quantification of

myocardial blood flow (MBF), the validated attenuation correction, and the superior image quality in obese patients [34, 35]. Three PET perfusion tracers have been established: ^{13}N ammonia ($^{13}NH_3$), ^{15}O water, and rubidium (^{82}Rb). $^{13}NH_3$, ^{15}O water, and ^{82}Rb have the advantage of a relatively short half-life, which is about 10 min for $^{13}NH_3$, 122 s for ^{15}O water, and 76 s for ^{82}Rb, which allows for rapid PET MPI scans in rest and under stress. Recently, ^{18}F flurpiridaz was introduced in early trials and has been shown to offer some advantages, e.g. a low positron energy and a half-life with the same logistical advantages as ^{18}F-FDG [36].

But despite the established role of PET MPI, myocardial perfusion imaging using dynamic contrast-enhanced (DCE-) MRI is a research since almost two decades and has shown promising results when compared to PET [5, 37, 38]. MRI perfusion imaging has a much greater availability than cardiac PET, a lower examination cost, and no ionizing radiation. MRI usually offers much greater spatial in-plane resolution than PET, enabling the possibility of voxel-wise quantitative perfusion analysis with a resolution of at least $2\times2\times8\text{mm}^3$ – although still at the price of limited LV coverage [39]. A spatial resolution of three to six slices per cardiac cycle can be achieved with reasonable SNR, surpassing the temporal capabilities of PET imaging. Independent of the competitive ambitions of MRI to take its share in the large market of diagnosing CAD, there is also great potential for integrated systems concerning the creation of synergies. To elucidate that potential, we briefly compare "perfusion" imaging as realized by both modalities.

For PET, the frame rate is usually in the order of 10 s, which is too low to actually observe the tracer's transit through the vascular space. Thus, PET MBF is estimated by observing tracer extraction from the vascular space into those parts of the myocardium where tracer kinetics are slow compared to the minimal frame rate. Retainable tracers as the ones listed above (with the exception of ^{15}O water) are indeed conceptually quite similar to microspheres [40], however adapted for noninvasive application. The main design criterion for those compounds is how efficiently they are extracted from the blood pool and transferred into the myocytes. Depending on the tracer, multi-compartmental modeling is used to map the diffusive extraction from the blood pool and subsequent retention inside the myocytes to simpler rate constants. From the specific model, a first-pass extraction flow constant (often called K_1) is calculated, which can be directly identified with MBF for freely diffusible tracers (^{15}O) or have to be corrected in case of high flow rates ($^{13}NH_3$, ^{82}Rb). In contrast, the underlying principle of myocardial MRI perfusion imaging is the direct observation of indicator convection through the vascular space, enabled by the high temporal resolution of MRI. The mathematical framework for that is the classic indicator-dilution theory as adapted for noninvasive applications by Zierler [41, 42]. This formalism, unlike compartment modeling, does not necessarily impose a priori physiological information about the structure of the tissue. Perfusion flow is described directly as the delivery amplitude of contrast media from the LV lumen (where the AIF is acquired) to the distribution volume of contrast agent in the myocardial tissue. Although rarely applied in myocardial perfusion studies, extraction-based approaches more similar to PET, e.g. the Tofts model [43], are still widely used in cerebral and oncologic studies. It is important to note though that for highly

vascularized tissue or high MBFs, the "extraction" of Gd-DTPA from the vascular space is permeability limited and not flow limited [44]. This renders it virtually impossible to extrapolate flow characteristics from Gd-DTPA extraction rates at high flows, which is why an extraction-based approach is usually not suitable for myocardial perfusion imaging at stress.

An additional, highly relevant point concerning MRI perfusion is that gadolinium-based contrast agents distribute in blood plasma, but do not permeate red blood cells (and thus the whole vascular space) as the more diffusible PET tracers do which clearly affects the generated signals (Fig. 3.5). As long as flow patterns of plasma

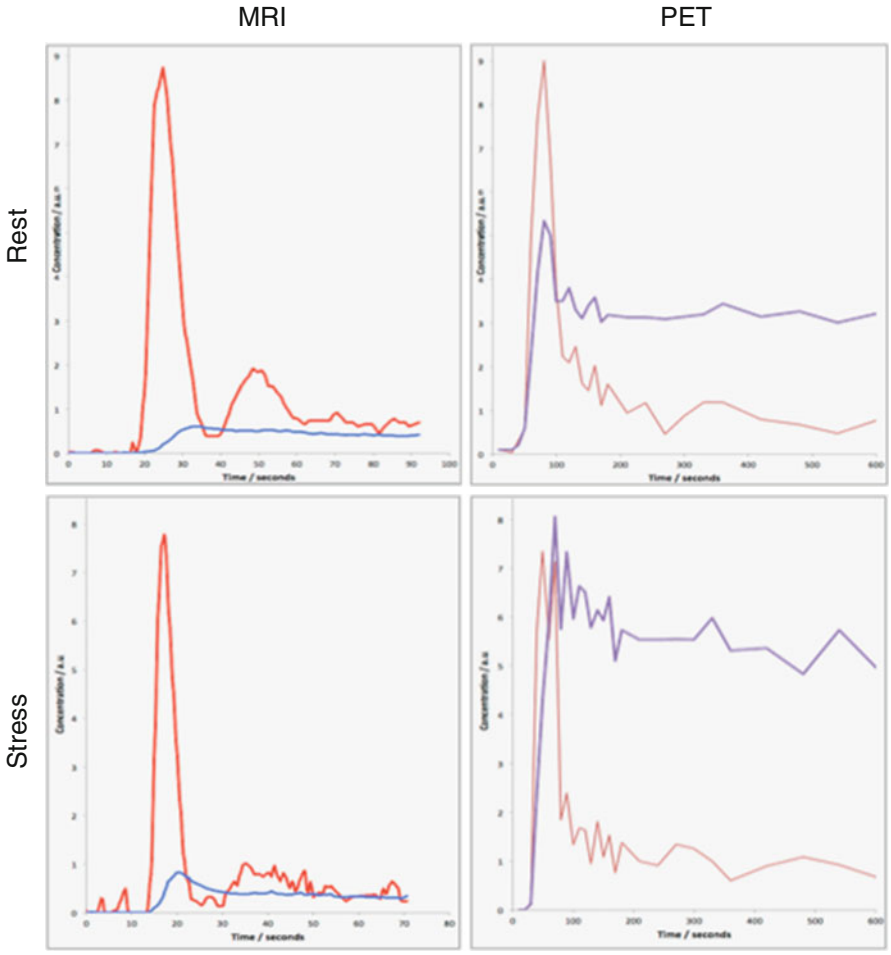

Fig. 3.5 Simultaneously acquired cardiac perfusion data. Curves are scaled arbitrarily to match peak input for improved visualization. The *red curves* show the left ventricular input functions and the *blue curves* display the tissue activity or Gd-DTPA concentrations, respectively. The different mechanisms of uptake into the cell (*PET*) or into the vascular and interstitial space (*MRI*) translate into clearly different amplitudes in the myocardial "tissue"

and blood cells are homogeneous, this has no influence on time-related parameters like mean indicator transit times (MTT). However, there is a need to correct for the effective difference between large-vessel hematocrit and microvascular hematocrit [45] when estimating MBF. This might affect especially stress studies [46, 47].

To which extent this has consequences in a clinical setup is unclear yet but might be one of the reasons for the per-patient variability seen in comparative studies [5]. There are several additional factors stemming from the need to accurately estimate contrast agent concentrations from MRI signal values, making data post processing much more complicated in PET. In a similar fashion as for hematocrit, those factors may affect input functions and tissue curves differently, e.g. water exchange conditions [48], Gd-DTPA relaxivity [49], AIF dispersion [50], and blood flow effects. In conclusion, despite important differences in data structure to PET, new opportunities arise from the spatially and temporally highly resolved assessment of microvascular dynamics from MRI-based flow assessments. Especially for integrated PET/MRI systems, such synergistic approaches hold great promise for future clinical applications in multimodal perfusion imaging.

3.3.2 Cardiac MRI for Tissue Characterization

Targeting the water and its properties is another technique modulating MRI to retrieve "molecular" information. In oncological imaging, using advanced imaging sequences and strong gradients, this avenue was already explored: the apparent diffusion coefficient (ADC) of water [51] is already widely used to characterize tumorous tissue. In general, water is the predominant source of the MR signal and its motility (or diffusion properties) can be used for tissue characterization. Another approach is the delineation of the longitudinal relaxation time T1. This parameter describes the potential of the exited spins to transfer their energy to the surrounding macromolecules. Thus, one of the changes in the microchemical cellular environment was the introduction of MR medical imaging as T1 values differ between healthy and tumorous tissue [52]. The so-called T1 weighting (and its modification, inversion recovery imaging) is still a fundamental imaging sequence in diagnosis imaging as different T1 values will produce different signal intensities, and thus, the contrast between healthy and abnormal tissue is optimized. For inversion recovery imaging, any signal from remote myocardium is nulled and scar tissue is enhanced in late gadolinium enhancement (LGE) [53]. More specifically, it shows areas with a different distribution volume for MR contrast agents. Accordingly, different washout kinetics from the interstitial space was shown previously in the acute as in the chronic setting of myocardial infarction [54, 55]. Unfortunately, larger clinical validations are still lacking, but two general modes of T1 mapping in the heart are already used in an increasing number of MRI centers. In the last decade, novel cardiac MR technology allowed the calculation of pixel-wise T1 maps [56]. Native T1 maps were used in imaging regional edema, fibrosis, amyloidosis, Anderson-Fabry disease, intramyocardial hemorrhage, and other structural alterations, where a modified water content and protein environment in the myocardium occurs [6].

In addition, using MR contrast media, pre- and post-contrast T1 maps enable the calculation of the extracellular volume (ECV). It was already shown that the expansion of extracellular matrix has prognostic value [57] and might have an important role in heart failure imaging. Even the term "vulnerable interstitium" was already coined in sudden death patients [58]. Although this is speculative, cardiac PET/MRI might be an excellent platform to validate and improve the characterization of myocardial tissue by integrating this information with tracer signals.

3.3.3 Improving Myocardial Tissue Characterization by 18F-FDG PET/MRI Viability Imaging

Myocardial hibernation is a well-known phenomenon where myocytes shift their metabolism from fatty acids toward glucose after chronic hypoperfusion [59]. Several preclinical and clinical studies have proved the beneficial effects of revascularization which is followed by recovery of the contractile function [60]. Several modalities showed potential to identify hibernating myocardium: dobutamine stress echocardiography, MRI, ^{18}F-FDG PET, and late gadolinium enhancement (LGE) MRI.

Considered as "gold standard" by many imagers, nuclear cardiology offers one of the most commonly applied techniques using ^{18}F-FDG PET as marker of myocardial viability [61]. Typically, ^{18}F-FDG is combined with a flow marker (^{13}N-ammonia, ^{82}Rb, and also ^{99m}Tc-labeled SPECT agents). Based on meta-analyses the sensitivity of ^{18}F-FDG PET to predict functional recovery after revascularization is about 92 %, while the specificity is only 63 % [62]. However, there is evidence that patients with a significant amount of dysfunctional but viable tissue should undergo revascularization as soon as possible as viability is a transient state of the myocytes [63, 64]. Especially from the point of view of spatial resolution, however, MRI offers with delayed gadolinium enhancement (LGE) a readily available approach. MRI spatial resolution is superior to PET (1–3 mm vs. 4–6 mm) which allows the differentiation between transmural and non-transmural infarction [65]. The same advantage helps with a reduced or absent ^{18}F-FDG uptake in thinned myocardium which would potentially be miscategorized as scar by PET. Despite these fundamental differences of the approaches (imaging viable vs. nonviable tissue), a good agreement between both modalities has been demonstrated in a chronic setting [53]. From a practical perspective, LGE is independent of the excretion of insulin and shows advantage in diabetic patients where the clearance of ^{18}F-FDG from the blood is limited and cardiac image quality is poor. However, if a hybrid use of ^{18}F-FDG PET MRI and LGE MRI is beneficial is still subject of research and only limited data is available indicating again good agreement (Fig. 3.6) [20].

In our initial experience in a similar setting, we found a small proportion of myocardial segments in disconcordance between ^{18}F-FDG uptake and transmurality of LGE [66]. However, the clinical relevance for functional recovery in the long-term setting post-acute MI is debatable and warrants further research.

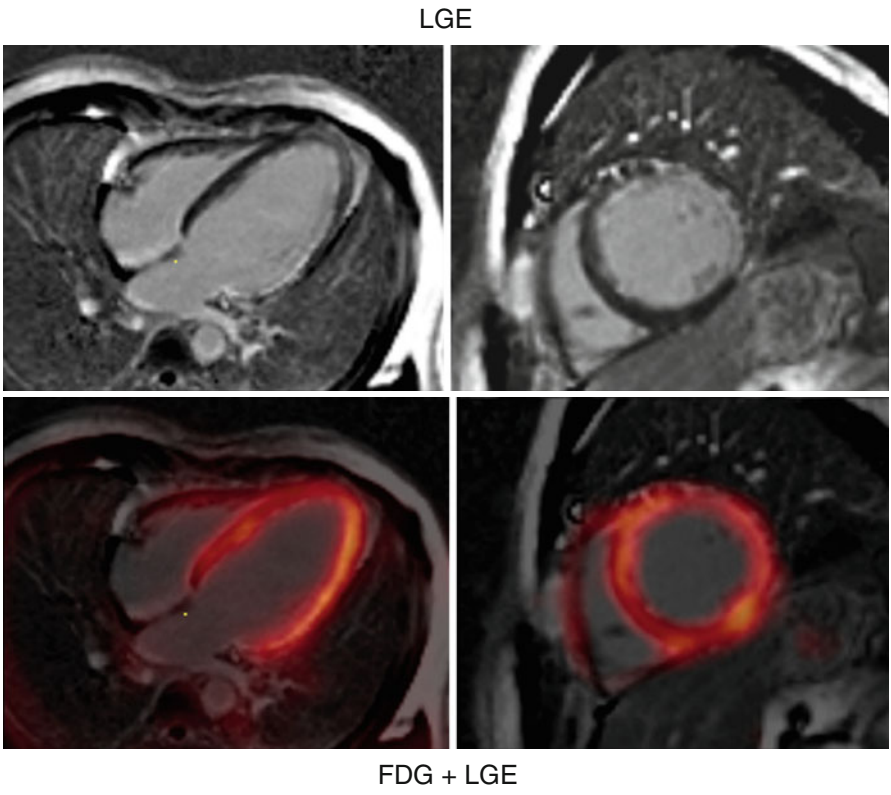

Fig. 3.6 18F-FDG PET/MRI shortly after AMI. Short- and long-axis images of a patient imaged shortly after acute MI with occlusion of the left main using simultaneous ^{18}F-FDG PET/MRI. In the *top row*, the LGE images and, in the *bottom row*, LGE images fused with FDG are shown

3.4 Applications in Cardiovascular Molecular Imaging: Targeting Inflammation

3.4.1 Inflammatory Response After Acute Myocardial Infarction

In the following paragraphs the delineation of (mostly) inflammatory signals is described in our first experience in distinct disease entities. Recent research has focused on the myocardial response to ischemia – with an emphasis on the cardiac inflammatory response after acute MI which is considered a risk factor for deleterious remodeling and finally the development of heart failure. The fact that monocytes migrate rapidly into the myocardium identified them as key components of cardiac inflammation [67–69]. This is a highly complex process and so far is the domain of preclinical research. However, ^{18}F-FDG PET – due to its readily availability – is frequently used in a variety of settings, as activated inflammatory cells show increased expression of glucose transporters which can be visualized

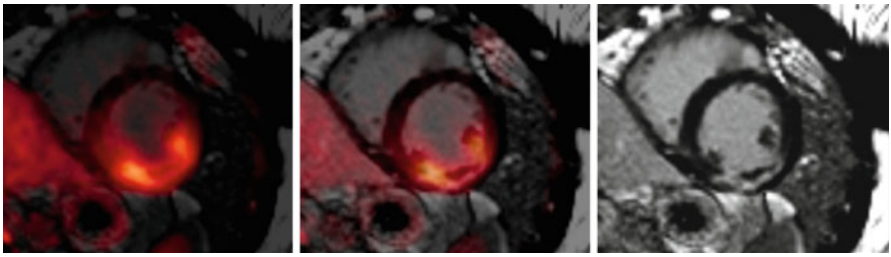

Fig. 3.7 Multimodal characterization of the myocardial tissue after AMI using PET/MRI. Short-axis images of a patient who was imaged shortly after acute MI using simultaneous ^{18}F-FDG PET/MRI. Myocardial scarring can be imaged using LGE MRI. Using fasted/heparin ^{18}F-FDG PET/MRI, the area of postischemic inflammation/ischemic memory can be assessed. Myocardial obstruction is visible at the center of the LGE zone

using ^{18}F-FDG PET. This signal could be supplemented with MRI's capability to image scar formation, microvascular obstruction, edema, hemorrhage, and left ventricular function. A recent preclinical study using a mouse infarct model of myocardial infarction showed that ^{18}F-FDG PET/MRI quantifies the amount of accumulated monocytes in the postischemic heart if the glucose uptake of cardiomyocytes is suppressed [70]. Such a strategy would enable a detailed morphologic characterization of the infarcted heart by PET/MRI and is feasible in humans (Fig. 3.7) [71, 72].

In patients, the glucose metabolism of cardiomyocytes can be suppressed by a high-fat/low-carb diet (the so-called Atkins diet) and/or the administration of unfractionated heparin prior to ^{18}F-FDG injection which is used, e.g., to image sarcoidosis with PET. However, there are limitations as the ^{18}F-FDG uptake is not unique in the heart: as used in conventional viability imaging, ischemically compromised myocardium switches its metabolism from fatty acids toward glucose degradation [73]. In addition, expression of GLUT1 transporters has been demonstrated in postischemic myocardium and can persist over weeks and is responsible for the "ischemic memory" [74, 75]. Thus, ^{18}F-FDG uptake in postischemic myocardium may not solely reflect inflammation but viable cardiomyocytes. However, if this characterization of tissue and its inflammatory state proves to be clinically reliable, it could identify patients at risk for developing heart failure or – even more relevant – it may serve as a tool to guide immunomodulatory therapeutic strategies.

3.4.2 Sarcoidosis

Following the same considerations as above, imaging inflammation in sarcoidosis developed into an attractive approach with PET/CT [76]. Sarcoidosis is a systemic granulomatous disease which is characterized by an intense inflammatory process and inflammatory granulomas, causing post-inflammatory scars. Those may result in conduction abnormalities, arrhythmia, and heart failure. Due to these large risks,

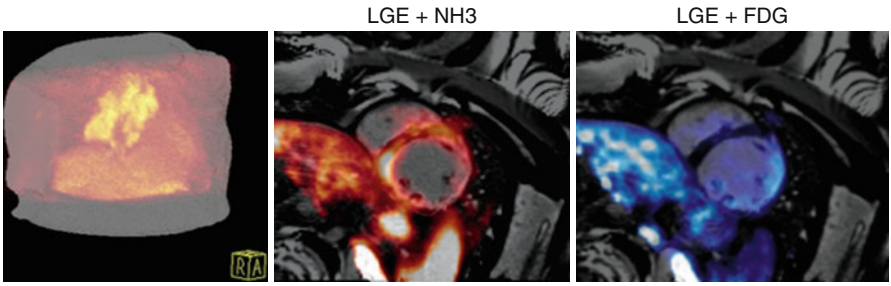

Fig. 3.8 Sarcoidosis. In a patient with acute sarcoidosis, a 3D rendering of the FDG uptake in the thorax (*left*), a fused LGE and NH3 perfusion PET (*middle*), and a fused LGE and FDG PET are depicted

cardiac involvement should be ruled out immediately. The guidelines of the Japanese Ministry of Health and Welfare, which serve as a worldwide standard, do currently not include PET but cardiac MRI or ^{67}Ga scintigraphy. In this particular setting, PET/MRI might be very useful for the initial diagnosis of cardiac sarcoidosis and also could guide therapy. As we showed initially, a combined approach of perfusion (e.g., ^{13}N-ammonia) and inflammation (e.g., ^{18}F-FDG), PET imaging would allow for exact staging of the disease as well as the assessment of the inflammatory status [77]: normal perfusion combined with avid ^{18}F-FDG uptake indicates active inflammation, hypoperfusion and intense glucose metabolism are suggestive for advanced stage, and reduced or absent perfusion and missing ^{18}F-FDG uptake are indicative for end-stage cardiac sarcoidosis. LGE MRI supplements the localization of regional fibrosis and aids the lead placement in the case of ICD implantation (Fig. 3.8).

3.4.3 Plaque Imaging in Atherosclerotic Disease

Finally, leaving the focus on imaging the heart, MRI is competing with CT in angiography if it comes to a characterization of the vessel wall, plaques, and their composition without the use of ionizing radiation [78, 79]. As an example from our group, Gd-contrast enhancement was observed in the vessel wall following myocardial infarction which correlated with the degree of stenosis and resolved in a 3-month follow-up scan possibly representing reduced inflammatory activity [80]. However, imaging the vessel wall requires substantial expertise and tends to be time-consuming. Thus, the combination with PET tracers could be attractive to facilitate imaging atherosclerotic plaques with a large spatial coverage. The dominating tracer is again ^{18}F-FDG, and it is assumed that an increased ^{18}F-FDG uptake is related to an intense macrophage infiltration representing a high vulnerability [81, 82]. Initial clinical work investigating the feasibility of simultaneous ^{18}F-FDG PET/MRI for imaging carotid arteries was demonstrated in six HIV-positive patients representing a population with a known increased risk of atherosclerosis [83]. Unfortunately, ^{18}F-FDG has limitations, and limited clearance from the blood pool

and uptake in muscle (including the heart itself) adjacent to the relatively small vessels are among them. Thus, the search for alternatives is ongoing. Recently, 80 patients with myocardial infarction were imaged with ^{18}F-fluoride (^{18}F-NaF) [84]. This tracer shows excellent imaging properties with clear focal uptake. In 93 % of the patients, the highest ^{18}F-NaF uptake was observed in the culprit lesion, while the ^{18}F-FDG uptake was obscured by the unspecific (muscular) myocardial uptake. Furthermore, almost every second patient with stable angina had plaques with focal ^{18}F-NaF uptake which were associated with high-risk features on intravascular ultrasound. Logistically, this agent is available and already in clinical (oncological) use. However, the evidence of usefulness is limited to a single study and future studies have to extend this. Potentially valuable tracers targeting integrins, such as $\alpha_V\beta_3$, have also been investigated in preclinical models and are currently being translated into clinics [85–87], and an initial study showed its feasibility in humans [88]. PET/MRI could also be an attractive platform for this very localized imaging as motion (both respiratory and cardiac) limits the detection. MRI could provide the means of motion detection and correction as already demonstrated in thoracic PET/MRI imaging [89, 90].

3.5 Summary

Today, both PET and MRI are well-recognized methods for the assessment of myocardial perfusion and viability. Integrating these modalities into a system capable of simultaneous acquisitions is a major technological achievement, but it remains to be seen whether this has a real added value in noninvasive cardiac imaging. At present cardiac PET/MRI is an attractive yet expensive research device with two focus areas: cross-validation of new imaging methods under identical experimental conditions and the search for synergistic applications. PET/MRI is currently slowly moving into clinical reality. The main reasons are the high costs, complex workflows, and the mandatory interdisciplinary interaction at a very high level. This results into the conclusion that it remains to be seen whether this new imaging technique is so cost-effective that cardiac imaging will profit from its unique and extraordinary capabilities.

References

1. Shaw LJ, Hendel R, Borges-Neto S, et al. Prognostic value of normal exercise and adenosine (99 m)Tc-tetrofosmin SPECT imaging: results from the multicenter registry of 4,728 patients. J Nucl Med. 2003;44(2):134–9.
2. Slomka PJ, Berman DS, Germano G. New cardiac cameras: single-photon emission CT and PET. Semin Nucl Med. 2014;44(4):232–51.
3. Kolh P, Windecker S. ESC/EACTS myocardial revascularization guidelines 2014. Eur Heart J. 2014;35(46):3235–6.
4. Gaemperli O, Kaufmann PA, Alkadhi H. Cardiac hybrid imaging. Eur J Nucl Med Mol Imaging. 2014;41 Suppl 1:S91–103.

5. Morton G, Chiribiri A, Ishida M, et al. Quantification of absolute myocardial perfusion in patients with coronary artery disease: comparison between cardiovascular magnetic resonance and positron emission tomography. J Am Coll Cardiol. 2012;60(16):1546–55.
6. Moon JC, Messroghli DR, Kellman P, et al. Myocardial T1 mapping and extracellular volume quantification: a Society for Cardiovascular Magnetic Resonance (SCMR) and CMR Working Group of the European Society of Cardiology consensus statement. J Cardiovasc Magn Reson. 2013;15:92.
7. Zaidi H, Ojha N, Morich M, et al. Design and performance evaluation of a whole-body Ingenuity TF PET-MRI system. Phys Med Biol. 2011;56(10):3091–106.
8. Delso G, Furst S, Jakoby B, et al. Performance measurements of the Siemens mMR integrated whole-body PET/MR scanner. J Nucl Med. 2011;52(12):1914–22.
9. Pichler BJ, Judenhofer MS, Catana C, et al. Performance test of an LSO-APD detector in a 7-T MRI scanner for simultaneous PET/MRI. J Nucl Med. 2006;47(4):639–47.
10. Davison H, Ter Voert EE, de Galiza Barbosa F, et al. Incorporation of time-of-flight information reduces metal artifacts in simultaneous positron emission tomography/magnetic resonance imaging: a Simulation Study. Invest Radiol. 2015 Mar 11 [Epub ahead of print]. doi:10.1097/RLI.0000000000000146.
11. Levin C, Deller T, Peterson W, Maramraju SH, Kim C, Prost R. Initial results of simultaneous whole-body ToF PET/MR. J Nucl Med. 2014;55(Supplement 1):660.
12. Martinez-Moller A, Souvatzoglou M, Navab N, Schwaiger M, Nekolla SG. Artifacts from misaligned CT in cardiac perfusion PET/CT studies: frequency, effects, and potential solutions. J Nucl Med. 2007;48(2):188–93.
13. Gould KL, Pan T, Loghin C, Johnson NP, Guha A, Sdringola S. Frequent diagnostic errors in cardiac PET/CT due to misregistration of CT attenuation and emission PET images: a definitive analysis of causes, consequences, and corrections. J Nucl Med. 2007;48(7):1112–21.
14. Souvatzoglou M, Bengel F, Busch R, et al. Attenuation correction in cardiac PET/CT with three different CT protocols: a comparison with conventional PET. Eur J Nucl Med Mol Imaging. 2007;34(12):1991–2000.
15. Koepfli P, Hany TF, Wyss CA, et al. CT attenuation correction for myocardial perfusion quantification using a PET/CT hybrid scanner. J Nucl Med. 2004;45(4):537–42.
16. Martinez-Moller A, Souvatzoglou M, Delso G, et al. Tissue classification as a potential approach for attenuation correction in whole-body PET/MRI: evaluation with PET/CT data. J Nucl Med. 2009;50(4):520–6.
17. Schulz V, Torres-Espallardo I, Renisch S, et al. Automatic, three-segment, MR-based attenuation correction for whole-body PET/MR data. Eur J Nucl Med Mol Imaging. 2011;38(1):138–52.
18. Fürst S, Souvatzoglu M, Rischpler C, Ziegler S, Schwaiger M, Nekolla S. Effects of MR contrast agents on attenuation map generation and cardiac PET quantification in PET/MR. J Nucl Med. 2012;53(Supplement 1):139.
19. Drzezga A, Souvatzoglou M, Eiber M, et al. First clinical experience with integrated whole-body PET/MR: comparison to PET/CT in patients with oncologic diagnoses. J Nucl Med. 2012;53(6):845–55.
20. Nensa F, Poeppel TD, Beiderwellen K, et al. Hybrid PET/MR imaging of the heart: feasibility and initial results. Radiology. 2013;268(2):366–73.
21. Nuyts J, Michel C, Fenchel M, Bal G, Watson C. Completion of a truncated attenuation image from the attenuated PET emission data. IEEE Trans Med Imaging. 2013;32(2):237–46. doi:10.1109/TMI.2012.2220376. Epub 2012 Sep 21.
22. Delso G, Martinez-Moller A, Bundschuh RA, Nekolla SG, Ziegler SI. The effect of limited MR field of view in MR/PET attenuation correction. Med Phys. 2010;37(6):2804–12.
23. Blumhagen JO, Ladebeck R, Fenchel M, Scheffler K. MR-based field-of-view extension in MR/PET: B(0) homogenization using gradient enhancement (HUGE). Magn Reson Med. 2013;70(4):1047–57.
24. Delso G, Martinez-Moller A, Bundschuh RA, et al. Evaluation of the attenuation properties of MR equipment for its use in a whole-body PET/MR scanner. Phys Med Biol. 2010; 55(15):4361–74.

25. Furst S, Souvatzoglou M, Martinez-Moller A, Schwaiger M, Nekolla SG, Ziegler SI. Impact of flexible body surface coil and patient table on PET quantification and image quality in integrated PET/MR. Nuklearmedizin (Nuclear medicine). 2014;53(3):79–87.
26. Paulus DH, Tellmann L, Quick HH. Towards improved hardware component attenuation correction in PET/MR hybrid imaging. Phys Med Biol. 2013;58(22):8021–40.
27. DiFilippo FP, Brunken RC. Do implanted pacemaker leads and ICD leads cause metal-related artifact in cardiac PET/CT? J Nucl Med. 2005;46(3):436–43.
28. Marinskis G, Bongiorni MG, Dagres N, Dobreanu D, Lewalter T, Blomstrom-Lundqvist C. Performing magnetic resonance imaging in patients with implantable pacemakers and defibrillators: results of a European Heart Rhythm Association survey. Europace. 2012;14(12):1807–9.
29. Cohen JD, Costa HS, Russo RJ. Determining the risks of magnetic resonance imaging at 1.5 tesla for patients with pacemakers and implantable cardioverter defibrillators. Am J Cardiol. 2012;110(11):1631–6.
30. Slomka PJ, Diaz-Zamudio M, Dey D, et al. Automatic registration of misaligned CT attenuation correction maps in Rb-82 PET/CT improves detection of angiographically significant coronary artery disease. J Nucl Cardiol. 2015 Feb 20 [Epub ahead of print]. doi:10.1007/s12350-014-0060-9.
31. Nekolla SG, Martinez-Moller A. Attenuation correction in cardiac PET: to raise awareness for a problem which is as old as PET/CT. J Nucl Cardiol. 2015 Feb 20 [Epub ahead of print]. doi:10.1007/s12350-015-0083-x.
32. Adluru G, Chen L, Kim SE, et al. Three-dimensional late gadolinium enhancement imaging of the left atrium with a hybrid radial acquisition and compressed sensing. J Magn Reson Imaging. 2011;34(6):1465–71.
33. Xue H, Zuehlsdorff S, Kellman P, et al. Unsupervised inline analysis of cardiac perfusion MRI. Med Image Comput Comput Assist Interv. 2009;12(Pt 2):741–9.
34. Flotats A, Bravo PE, Fukushima K, Chaudhry MA, Merrill J, Bengel FM. (82)Rb PET myocardial perfusion imaging is superior to (99 m)Tc-labelled agent SPECT in patients with known or suspected coronary artery disease. Eur J Nucl Med Mol Imaging. 2012;39(8):1233–9.
35. Murthy VL, Di Carli MF. Non-invasive quantification of coronary vascular dysfunction for diagnosis and management of coronary artery disease. J Nucl Cardiol. 2012;19(5):1060–72.
36. Sinusas AJ, Lazewatsky J, Brunetti J, et al. Biodistribution and radiation dosimetry of LMI1195: first-in-human study of a novel 18F-labeled tracer for imaging myocardial innervation. J Nucl Med. 2014;55(9):1445–51.
37. Schwitter J, Nanz D, Kneifel S, et al. Assessment of myocardial perfusion in coronary artery disease by magnetic resonance: a comparison with positron emission tomography and coronary angiography. Circulation. 2001;103(18):2230–5.
38. Ibrahim T, Nekolla SG, Schreiber K, et al. Assessment of coronary flow reserve: comparison between contrast-enhanced magnetic resonance imaging and positron emission tomography. J Am Coll Cardiol. 2002;39(5):864–70.
39. Hsu LY, Groves DW, Aletras AH, Kellman P, Arai AE. A quantitative pixel-wise measurement of myocardial blood flow by contrast-enhanced first-pass CMR perfusion imaging: microsphere validation in dogs and feasibility study in humans. JACC Cardiovasc Imaging. 2012;5(2):154–66.
40. Domenech RJ, Hoffman JI, Noble MI, Saunders KB, Henson JR, Subijanto S. Total and regional coronary blood flow measured by radioactive microspheres in conscious and anesthetized dogs. Circ Res. 1969;25(5):581–96.
41. Zierler KL. Equations for measuring blood flow by external monitoring of radioisotopes. Circ Res. 1965;16:309–21.
42. Zierler K. Indicator dilution methods for measuring blood flow, volume, and other properties of biological systems: a brief history and memoir. Ann Biomed Eng. 2000;28(8):836–48.
43. Tofts PS. Modeling tracer kinetics in dynamic Gd-DTPA MR imaging. J Magn Reson Imaging. 1997;7(1):91–101.

44. Sourbron SP, Buckley DL. On the scope and interpretation of the Tofts models for DCE-MRI. Magn Reson Med. 2011;66(3):735–45.
45. Klitzman B, Duling BR. Microvascular hematocrit and red cell flow in resting and contracting striated muscle. Am J Physiol. 1979;237(4):H481–90.
46. Brands J, van Haare J, Vink H, Vanteeffelen JW. Whole-body recruitment of glycocalyx volume during intravenous adenosine infusion. Physiol Rep. 2013;1(5), e00102.
47. Eliasen P, Amtorp O. Effect of intracoronary adenosine upon regional blood flow, microvascular blood volume and hematocrit in canine myocardium. Int J Microcirc Clin Exp. 1984;3(1):3–12.
48. Donahue KM, Burstein D, Manning WJ, Gray ML. Studies of Gd-DTPA relaxivity and proton exchange rates in tissue. Magn Reson Med. 1994;32(1):66–76.
49. Stanisz GJ, Henkelman RM. Gd-DTPA relaxivity depends on macromolecular content. Magn Reson Med. 2000;44(5):665–7.
50. Calamante F, Gadian DG, Connelly A. Delay and dispersion effects in dynamic susceptibility contrast MRI: simulations using singular value decomposition. Magn Reson Med. 2000;44(3):466–73.
51. Vag T, Heck MM, Beer AJ, et al. Preoperative lymph node staging in patients with primary prostate cancer: comparison and correlation of quantitative imaging parameters in diffusion-weighted imaging and 11C-choline PET/CT. Eur Radiol. 2014;24(8):1821–6.
52. Damadian R, Zaner K, Hor D, DiMaio T, Minkoff L, Goldsmith M. Nuclear magnetic resonance as a new tool in cancer research: human tumors by NMR. Ann N Y Acad Sci. 1973;222:1048–76.
53. Klein C, Nekolla SG, Bengel FM, et al. Assessment of myocardial viability with contrast-enhanced magnetic resonance imaging: comparison with positron emission tomography. Circulation. 2002;105(2):162–7.
54. Klein C, Nekolla SG, Balbach T, et al. The influence of myocardial blood flow and volume of distribution on late Gd-DTPA kinetics in ischemic heart failure. J Magn Reson Imaging. 2004;20(4):588–93.
55. Klein C, Schmal TR, Nekolla SG, Schnackenburg B, Fleck E, Nagel E. Mechanism of late gadolinium enhancement in patients with acute myocardial infarction. J Magn Reson Imaging. 2007;9(4):653–8.
56. Messroghli DR, Radjenovic A, Kozerke S, Higgins DM, Sivananthan MU, Ridgway JP. Modified Look-Locker inversion recovery (MOLLI) for high-resolution T1 mapping of the heart. J Magn Reson Imaging. 2004;52(1):141–6.
57. Wong TC, Piehler KM, Kang IA, et al. Myocardial extracellular volume fraction quantified by cardiovascular magnetic resonance is increased in diabetes and associated with mortality and incident heart failure admission. Eur Heart J. 2014;35(10):657–64.
58. Tamarappoo BK, John BT, Reinier K, et al. Vulnerable myocardial interstitium in patients with isolated left ventricular hypertrophy and sudden cardiac death: a postmortem histological evaluation. J Am Heart Assoc. 2012;1(3), e001511.
59. Ghosh N, Rimoldi OE, Beanlands RS, Camici PG. Assessment of myocardial ischaemia and viability: role of positron emission tomography. Eur Heart J. 2010;31(24):2984–95.
60. Di Carli MF. Predicting improved function after myocardial revascularization. Curr Opin Cardiol. 1998;13(6):415–24.
61. Tillisch J, Brunken R, Marshall R, et al. Reversibility of cardiac wall-motion abnormalities predicted by positron tomography. N Engl J Med. 1986;314(14):884–8.
62. Schinkel AF, Poldermans D, Elhendy A, Bax JJ. Assessment of myocardial viability in patients with heart failure. J Nucl Med. 2007;48(7):1135–46.
63. Bax JJ, Schinkel AF, Boersma E, et al. Early versus delayed revascularization in patients with ischemic cardiomyopathy and substantial viability: impact on outcome. Circulation. 2003;108 Suppl 1:II39–42.
64. Beanlands RS, Ruddy TD, deKemp RA, et al. Positron emission tomography and recovery following revascularization (PARR-1): the importance of scar and the development of a prediction rule for the degree of recovery of left ventricular function. J Am Coll Cardiol. 2002;40(10):1735–43.

65. Kim RJ, Wu E, Rafael A, et al. The use of contrast-enhanced magnetic resonance imaging to identify reversible myocardial dysfunction. N Engl J Med. 2000;343(20):1445–53.
66. Rischpler C, Langwieser N, Souvatzoglou M, et al. PET/MRI early after myocardial infarction: evaluation of viability with late gadolinium enhancement transmurality vs. 18F-FDG uptake. Eur Heart J Cardiovasc Imaging. 2015;16(6):661–9. doi:10.1093/ehjci/jeu317. Epub 2015 Feb 13.
67. Frangogiannis NG, Smith CW, Entman ML. The inflammatory response in myocardial infarction. Cardiovasc Res. 2002;53(1):31–47.
68. Maekawa Y, Anzai T, Yoshikawa T, et al. Prognostic significance of peripheral monocytosis after reperfused acute myocardial infarction: a possible role for left ventricular remodeling. J Am Coll Cardiol. 2002;39(2):241–6.
69. Nahrendorf M, Swirski FK, Aikawa E, et al. The healing myocardium sequentially mobilizes two monocyte subsets with divergent and complementary functions. J Exp Med. 2007;204(12):3037–47.
70. Lee WW, Marinelli B, van der Laan AM, et al. PET/MRI of inflammation in myocardial infarction. J Am Coll Cardiol. 2012;59(2):153–63.
71. Wollenweber T, Roentgen P, Schafer A, et al. Characterizing the inflammatory tissue response to acute myocardial infarction by clinical multimodality noninvasive imaging. Circ Cardiovasc Imaging. 2014;7(5):811–8.
72. Rischpler C, Nekolla SG, Dregely I, Schwaiger M. Hybrid PET/MR imaging of the heart: potential, initial experiences, and future prospects. J Nucl Med. 2013;54(3):402–15.
73. Schwaiger M, Schelbert HR, Ellison D, et al. Sustained regional abnormalities in cardiac metabolism after transient ischemia in the chronic dog model. J Am Coll Cardiol. 1985;6(2):336–47.
74. Egert S, Nguyen N, Schwaiger M. Myocardial glucose transporter GLUT1: translocation induced by insulin and ischemia. J Mol Cell Cardiol. 1999;31(7):1337–44.
75. Taegtmeyer H, Dilsizian V. Imaging myocardial metabolism and ischemic memory. Nat Clin Pract Cardiovasc Med. 2008;5 Suppl 2:S42–8.
76. Blankstein R, Osborne M, Naya M, et al. Cardiac positron emission tomography enhances prognostic assessments of patients with suspected cardiac sarcoidosis. J Am Coll Cardiol. 2014;63(4):329–36.
77. Schneider S, Batrice A, Rischpler C, Eiber M, Ibrahim T, Nekolla SG. Utility of multimodal cardiac imaging with PET/MRI in cardiac sarcoidosis: implications for diagnosis, monitoring and treatment. Eur Heart J. 2014;35(5):312.
78. Fayad ZA, Fuster V, Fallon JT, et al. Noninvasive in vivo human coronary artery lumen and wall imaging using black-blood magnetic resonance imaging. Circulation. 2000;102(5):506–10.
79. Kim WY, Stuber M, Bornert P, Kissinger KV, Manning WJ, Botnar RM. Three-dimensional black-blood cardiac magnetic resonance coronary vessel wall imaging detects positive arterial remodeling in patients with nonsignificant coronary artery disease. Circulation. 2002;106(3):296–9.
80. Ibrahim T, Makowski MR, Jankauskas A, et al. Serial contrast-enhanced cardiac magnetic resonance imaging demonstrates regression of hyperenhancement within the coronary artery wall in patients after acute myocardial infarction. JACC Cardiovasc Imaging. 2009;2(5):580–8.
81. Rudd JH, Warburton EA, Fryer TD, et al. Imaging atherosclerotic plaque inflammation with [18F]-fluorodeoxyglucose positron emission tomography. Circulation. 2002;105(23):2708–11.
82. Davies JR, Rudd JH, Weissberg PL, Narula J. Radionuclide imaging for the detection of inflammation in vulnerable plaques. J Am Coll Cardiol. 2006;47(8 Suppl):C57–68.
83. Ripa RS, Knudsen A, Hag AM, et al. Feasibility of simultaneous PET/MR of the carotid artery: first clinical experience and comparison to PET/CT. Am J Nucl Med Mol Imaging. 2014;4(5):448–58.
84. Joshi NV, Vesey AT, Williams MC, et al. 18F-fluoride positron emission tomography for identification of ruptured and high-risk coronary atherosclerotic plaques: a prospective clinical trial. Lancet. 2014;383(9918):705–13.

85. Saraste A, Laitinen I, Weidl E, et al. Diet intervention reduces uptake of alphavbeta3 integrin-targeted PET tracer 18F-galacto-RGD in mouse atherosclerotic plaques. J Nucl Cardiol. 2012;19(4):775–84.
86. Laitinen I, Notni J, Pohle K, et al. Comparison of cyclic RGD peptides for alphavbeta3 integrin detection in a rat model of myocardial infarction. EJNMMI Res. 2013;3(1):38.
87. Beer AJ, Pelisek J, Heider P, et al. PET/CT imaging of integrin alphavbeta3 expression in human carotid atherosclerosis. JACC Cardiovasc Imaging. 2014;7(2):178–87.
88. Makowski MR, Ebersberger U, Nekolla S, Schwaiger M. In vivo molecular imaging of angiogenesis, targeting alphavbeta3 integrin expression, in a patient after acute myocardial infarction. Eur Heart J. 2008;29(18):2201.
89. Furst S, Grimm R, Hong I, et al. Motion correction strategies for integrated PET/MR. J Nucl Med. 2015;56(2):261–9.
90. Grimm R, Furst S, Souvatzoglou M, et al. Self-gated MRI motion modeling for respiratory motion compensation in integrated PET/MRI. Med Image Anal. 2015;19(1):110–20.